The non-destructive characterization of a rare Liao silver reliquary from the Museum of oriental art in Turin (Italy)

Journal of Cultural Heritage 75 (2025) 23–30

Contents lists available at ScienceDirect

Journal of Cultural Heritage

journal homepage: www.elsevier.com/locate/culher

Case study

The non-destructive characterization of a rare Liao silver reliquary from the Museum of oriental art in Turin (Italy)

Benedetta Vitale[a,*], Giancarlo Cicero[b], Emma Angelini[b], Sabrina Grassini[b], Gaia Platania[b], Micaela Castellino[b], Marco Fontana[b], Tommaso Poli[a], Anna Collarin[c], Marco Demmelbauer[c], Franca Varallo[e], Stefania De Blasi[c], Marco Guglielminotti Trivel[d], Eliano Diana[a]

[a] Department of Chemistry, University of Turin, Via Giuria 7, Turin 10125, Italy
[b] Department of Applied Science and Technology, Politecnico di Torino, Corso Duca degli Abruzzi 24, Turin 10129, Italy
[c] Fondazione Centro Conservazione e Restauro "La Venaria Reale", Venaria Reale, 10078 Turin, Italy
[d] Formerly Museum of Oriental Art (MAO), Via San Domenico 11, Turin 10122, Italy
[e] Department of Historical Studies, University of Turin, Via Sant'Ottavio 20, Turin 10124, Italy

ARTICLE INFO

Article history:
Received 22 March 2025
Accepted 8 July 2025
Available online 19 July 2025

Keywords:
Liao dynasty
Chinese reliquary
Silver embrittlement
X-ray photoelectron spectroscopy

ABSTRACT

The present research study focuses on the archaeometric investigation of a delicate silver object. The artefact may be stylistically attributed to the Chinese Liao dynasty (907–1125 AD) and exhibits some peculiar aspects. It is made up of five overlapping and untied silver foil components, which may have been taken from unrelated artefacts and reassembled in ancient times. However, very little provenance information is available, and its manufacturing process is unknown. In addition, the reliquary was found in a highly fragmentary state, with advanced corrosion, extensive yellowing of the silver foils and severe embrittlement, which highly compromised its structural integrity and the legibility of its decorative features. Thus, a non-destructive and multi-analytical approach, based on surface spectroscopic techniques and structural characterization, was carried out on micro-fragments detached spontaneously from the reliquary. This study investigates the materials and manufacturing techniques, the conservation history, and the coherence of the five assembled components of this unique reliquary. Moreover, the investigation allowed us to gain insight into the silver microstructure and the possible causes of the observed alteration phenomena The results provide new knowledge on the metalworking practices of the Liao dynasty and might be valuable for developing and optimising strategies to restore the structural integrity of brittle ancient silver artefacts.

Introduction and research aims

Buddhism was introduced to China from India and Central Asia and flourished during the Tang dynasty (AD 618–907). However, in the mid-9th century, temples were dismantled, and holy artefacts were smashed during a violent repression. Soon after, Buddhism was restored, and, under the Liao dynasty (AD 907–1125), reliquaries still played an important role [1]. Since the 1950s, nearly 100 sites containing Buddhist relics from the Northern Song dynasty (AD 960–1127) and the Liao dynasty have been excavated in China. Many reliquaries have been preserved in relatively good condition and often bear inscriptions relating to the dates and occasions of the burial [2,3]. In particular, Buddhist reliquaries from the late Tang and Liao dynasties appeared as miniature pagodas, usually placed in several nested boxes, wrapped in thin silk, and decorated with Buddhist images on the lids [4,5].

The present study focuses on a delicate Chinese silver reliquary[1] preserved in the Museum of Oriental Art, *Museo d'Arte Ori-*

Abbreviations: XPS, X-ray photoelectron spectroscopy; SEM-EDS, Scanning electron microscopy coupled with energy-dispersive X-ray spectroscopy; SEM-BSE, Scanning electron microscopy - Back-scattered electrons; XRPD, X-ray powder diffraction; XRF, XRay Fluorescence spectroscopy; UV, Ultraviolet photography; FTIR, Fourier transform infrared spectroscopy.

* Corresponding author.
E-mail address: benedetta.vitale@unito.it (B. Vitale).

[1] We refer to the examined artefact as a 'reliquary' because it has been handed down with this term and because of its aesthetic features. However, in its current state, it is not a proper relics container; rather, it resembles a model pagoda, likely of a votive type.

https://doi.org/10.1016/j.culher.2025.07.013

entale (MAO), in Turin, Italy. Allegedly, it has been attributed to the Liao period [6]. The reliquary has little information on provenance, burial conditions, context of the discovery, and previous restorations. It was in a poor conservation state, with severe embrittlement, loss of structural integrity, and yellow-brown appearance of the foils.

In ancient silver artefacts, copper was deliberately added for economic reasons and to increase strength and wear resistance [7]. However, copper precipitation in silver alloy can be one of the causes of corrosion and embrittlement. Specifically, different embrittlement mechanisms have been reported in the literature: i. intergranular corrosion in mechanically worked and annealed finds; ii. synergistic corrosion-induced (transgranular) and microstructural (intergranular) embrittlement, in case of a significant amount of retained cold work [8,9].

Although several sophisticated Tang and Liao gold and silver artefacts were excavated, technical characteristics of ancient East Asian silver reliquaries have rarely been discussed [10,11]. As a result, there is a knowledge gap in material composition and execution techniques. Understanding the type of alloy, manufacture, nature, and extent of the embrittlement is essential not only for retrieving information on the original alloy and the burial and conservation environments, but also for optimizing restoration methodologies.

The present work investigates the composition, structure, and state of conservation by non-destructive complementary methods. Surface-sensitive spectroscopic techniques, such as X-ray photoelectron spectroscopy (XPS) and Scanning Electron Microscopy (SEM), and structural characterization by X-ray powder diffraction (XRPD) were carried out on micro-fragments, which spontaneously detached from the highly brittle reliquary. The results could be extremely valuable for establishing the most appropriate restoration treatments and enhancing the understanding of metalworking practices in the Liao dynasty. In addition, some preliminary clues about the possible coherence of the five assembled have been highlighted.

Materials and methods

Description of the reliquary

The present reliquary is a miniature octagonal pagoda (h x w: 43 × 22 cm) stylistically attributed to the Liao dynasty. It was acquired in 1997 by the Fondazione Giovanni Agnelli (Turin, Italy) from an antique shop in Hong Kong (called “Ngai Yuen” or “Yu Fa Ko Ngai Yuen”). Then, it was acquired by Fondazione per l’Arte e la Cultura della Compagnia di San Paolo (a banking foundation in Turin) to increase the collections of the Museum of Oriental Art (MAO) of Turin, opened to the public in 2008. Since 2008, it has been conserved in the museum storerooms at 19/24 °C and about 45 % RH. No previous conservation treatments were recorded [12]. In 2019, the reliquary was chosen as an object of interest for a master’s thesis in conservation and restoration of cultural heritage at the University of Turin and the La Venaria Reale Conservation and Restoration Centre.

The reliquary consists of five overlapping and untied components: three elements on the base, the central body as the fourth piece, the roof with a pole holding a parasol and a globe as the fifth component (Fig. 1).

The first component shows a *horror vacui* vegetable motif standing out from the punched background, which was common in Tang metalwork [13]. At the edges, there are two mirrored “S” motifs with side-punched circles, vertical repoussé lines and chisel marks.

The rise of the first tier shows a fretworked cloud with two lateral repoussé clouds. The same motif was identified on the Liao gilded silver set found in the Qingzhou White Pagoda [14] (*Fig. S2*).

The ridge of the second tier shows continuous wavy phytomorphic motifs, also found on the silver reliquary excavated from a pagoda of the Jingzhong Monastery (Northern Song dynasty) [4]. The treads of the first and second tiers show floral decoration and phytomorphic motifs. The chisel marks were observed under lateral grazing light (*Fig. S3*)

The second component consists of three horizontal tiers with plants and lotus leaf decorations, also found in a silver box excavated from the Buddhist Famen Temple [15]. A repoussé winged animal motif was identified on the third level, probably depicting exotic parakeets, animals used as tribute gifts in the Tang times (*Fig. S4*) [16].

The third component has a lower octagonal base with chamfered edges; each side shows a stylized lotus leaf and floral ornaments, which were not observed in the other reliquary components. The upper part consists of two embossed levels of lotus petals (*Fig. S5*).

The central body (the fourth reliquary component) is a repoussé architectural system framing the eight faces of the pagoda: one depicting a slightly opened door, the two faces flanking the door showing armed guardians amid plants, the remaining five faces with five different figures wearing long robes that were not identified. Moreover, the central body does not show depictions of Buddhist deities, which is quite unusual for this type of reliquary [4] (*Fig. S6*).

A connecting element with simple geometric decorative motifs joins the body to the roof. The ends of this piece were joined by silver stitching (*Fig. S6*).

The roof has a grooved profile with five sloping levels and a spherical cap with lotus petals arranged in a sunburst pattern. On the top, a pole holds a parasol and a deep-drawn metal globe fixed with silver threads. The pole appears to be unrelated to the other components because of its colour and diameter, which is larger than those of the lower and upper inserted fragments (*Fig. S7*).

Eight dragon-shaped gutters were probably attached to the ends of the roof with silver thread. Traces of small rings are in the holes representing the dragon’s eyes (*Fig. S8*). Considering similar reliquaries, one could deduce that small chains supported bud-shaped bells [2].

Regarding the execution techniques, the tool marks suggest that the central body was cold-forged to form an octagonal prism and the ends were stitched together with silver threads. The base and roof were hammered from a single foil sheet, since fine engravings related to the hammering process were observed on the edges of the first and second elements. The engraving was probably made on the parent sheet to mark the edge positions, which were later produced during the shaping and hammering tiers. More specifically, the slightly curved shapes of the foils, the localization of the cracks at the edges, and the greater thickness of the outer zones may be distinctive of a process similar to the deep drawing [17] (*Fig. S9*).

Samples

Six micro-fragments (s1, s2, s3, s4, s5, s6) and six fragments (a, b, c, d, e, f) spontaneously detached were analysed. s4 is from the first component; a and b are from the second piece; s5, s6, c, d, and e are from the third element; s1, s2, s3, and f are from the fourth component (the central body) (Fig. 1, Table S1).

Characterization techniques

- Optical microscopy: Leica MZFLII microscope with a digital camera was used to examine the tool marks, textile traces, and cracking profile.

Fig. 1. The reliquary studied in the present work (h x w: 43 × 22 cm) and the five untied components. First and second pieces: the two components of the base; third component: the lotus-leaf-motif piece; fourth component: the central body; fifth component: the roof with the pole bearing the parasol and the globe.

- Ultraviolet photography (UV) was employed to identify restoration materials. The lighting was achieved using two 5-W Madatec LED UV (emission peak at 368 nm), four Labino UV light MPXL and UV Floodlight spot lamps (emission peak at 365 nm). Images were acquired in the 380–780-nm range with a Nikon D810 DSLR Full Spectrum camera, modified to extend its sensitivity in the 350–1000-nm range, providing a resolution of 7360 × 4912 pixels, equipped with a metal oxide semiconductor silicon sensor, Madatec UV-IR Cut, BG40 filters, and a polarizer. Image processing was performed on PTGui software.
- X-Ray Fluorescence (XRF): qualitatively analyse of the alloy was conducted with a micro-XRF Bruker Artax 200 spectrometer (Mo anode, Si(Li) detector, 8-μm Be window), 50 kV, and maximum 1500 µA.
- Fourier transform infrared spectroscopy (FTIR): it was performed to characterize yellowing substances, tissue remains, corrosion products and fillers, with a Bruker Vertex 70 FTIR spectrometer, equipped with Hyperion 3000 microscope and MCT detector (4000–650 cm^{-1} range, 4 cm^{-1} resolution, 64 scans for each spectrum). Scrapings were analysed as bulk in transmission, upon compression in a diamond anvil cell.
- Field Emission Scanning Electron Microscopy coupled with Oxford Energy Dispersive X-ray Spectroscopy (FE-SEM-EDS) was used for the morphological and elemental analysis of the fragments (working distance: 5 mm; acceleration voltages: 5 and 20 kV). SEM images in Fig. 3 were acquired by Zeiss EVO60 (LaB_6 cathode), with an Oxford Ultim Max EDS probe.
- X-ray Powder Diffraction (XRPD): the crystalline phases on the micro-fragments were characterized by the PANalytical X'Pert Pro X-ray instrument Cu-Kα (λ=1.5418 Å) in the Bragg-Brentano geometry (accumulation time: 75–150 s; angular range: 2θ = 10°- 90°; step: 0.026°), using the associated software for the phase identification.
- X-ray Photoelectron Spectroscopy (XPS): areas of interest were analysed with PHI 5000 Versa Probe spectrometer (Al Kα excitation source, 1486.6 eV, scan area: 100 × 100 μm^2). After survey scans, High-Resolution (HR) scans were collected for relevant Au, Ag, and Pb peaks.

Results and discussion

Characterization of previous restoration materials

UV light examination revealed bluish-fluorescent materials, particularly at the pole extremities (*Fig. S10*), identified as poly-ethyl cyanoacrylates by FTIR (−3490 cm^{-1}: OH stretching; 2970, 2940, 2880 cm^{-1}:CH_2- stretching; 2250 cm^{-1}:CN stretching; 1460, 1380 cm^{-1}:CH_2- bending; 1250, 1170 cm^{-1}:COO- stretching; 1040 cm^{-1}:C-O- stretching; 980 cm^{-1}:CH_2- bending (spectrum *j* in *Fig. S12, Table S2*) [18]. The presence of poly-ethyl cyanoacrylates suggests that they were likely applied in modern times as adhesive agents to bond the pole to the roof and globe.

Some areas of the silver foil show extensive yellowing and amber-coloured deposits, identified as terpenoid resins by FTIR (3400 cm^{-1}: OH stretching; 2960, 2890 cm^{-1}:CH_2- stretching; 1740 cm^{-1}:C=O stretching; 1400, 1380, 1250 cm^{-1}:CH_2- and OH bending, C–O stretching in phenols; 1170 cm^{-1}:COO- stretching in esters; 1100 cm^{-1}: aromatic C–H bending (*Fig. S13* and spectrum *f* in *Fig. S12, Table S2*) [19]. Therefore, the yellowing of the silver foil is due to the photo-oxidative degradation of resins applied as protective coatings. However, under UV light, the surface shows only small residues and lacks the expected general fluorescence emission, likely because cupper compounds absorb the emitted fluorescence [20].

The amber resin on the micro-fragments (s1-s6) was investigated by SEM-EDS and XPS. SEM images show non-uniform resin distributions, with atomic C/O ratios of ∼4. On s1 chloride traces were detected by microanalysis, but not by XPS. The analytical volume of EDS is thicker than the ten-nanometre depth probed by XPS. Thus, chloride-bearing degradation products may be under the resin, probably applied as protective coatings where the corrosion process had already started (*Fig. S13*).

Textile traces

Mineralized textile remains were found on the body, first, third, and connecting pieces (*Fig. S14a*). They show a plain weave with 22–24 wefts/cm and 34–36 warps/cm, resembling canvas or taffeta, consistent with the Liao custom of wrapping reliquaries in thin silk [21]. Instead, the first component displays a different plant tissue than that of the other pieces, with 30 warps and 30 wefts/cm.

The textile remains were analysed by FTIR to determine the original composition of the tissue and detect any possible inorganic compounds present as contaminants or pigments (*Fig. S14a*). The resulting spectra show only the diagnostic signals of basic lead carbonate ($(PbCO_3)_2{\cdot}Pb(OH)_2$), suggesting that the textile underwent complete mineralization (3400 cm^{-1}: OH stretching; 1740 cm^{-1}: C=O stretching; 1450 cm^{-1}: CO_3^{2-} asymmetric stretching; 1050 cm^{-1}: CO_3^{2-} symmetric stretching; 850 cm^{-1}: CO_3^{2-} -out-of-plane bending; 690 cm^{-1}: CO_3^{2-} in-plane bending (spectrum *i* in *Fig. S12, Table S2*) [22]. This finding indicates the possible migration of Pb^{2+} ions from the reliquary alloy into the tissue, combined with the organic decomposition of the textile, resulting in the nucleation of inorganic phases, such as lead carbonates. Basic lead carbonates may also form through interactions with environmental factors, like humidity and carbonate-rich soil [23].

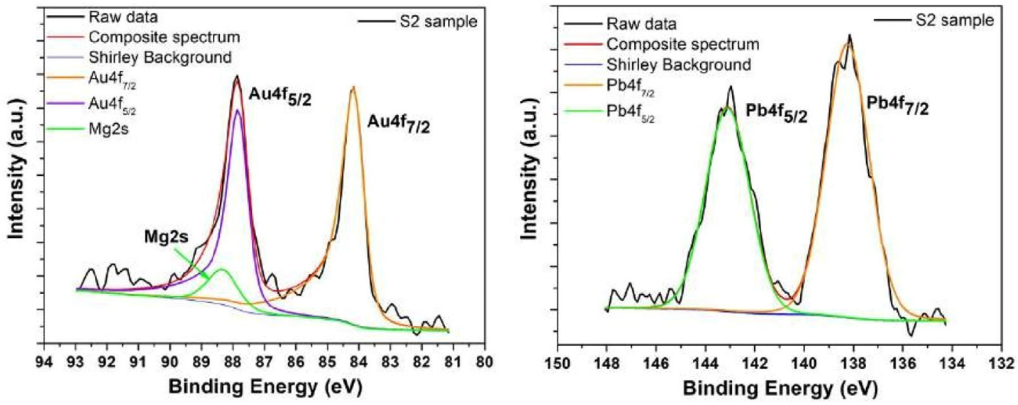

Fig. 2. High-resolution Au 4f XPS spectrum (on the left) and Pb 4f XPS spectrum (on the right) of the micro-fragment s2 (front side) after the laser cleaning.

Alloy composition and microstructure

XRF results are reported in *Fig. S15* and *Table S3*: the reliquary components mainly consist of Ag/Cu alloy. Only the pole and its extremities are composed of Cu alloy.

The micro-fragments (s1-s6) were further characterized by SEM and XPS. SEM images of s1, s2, and s3 reveal coarse, patchy surfaces, with submicrometric rounded particles agglomerated to form small clumps. In contrast, *s4* and *s5* exhibit compact and smooth surfaces (*Fig. S16*).

The average Cu content detected by SEM-EDS ranges from 0.4 % to 2.4 % at., except *s3*, which exhibits higher Cu contents (~4 % at.). Ag ranges between 14 and 34 % at.

As shown by standard deviations in Table 1, there are significantly large content variations in the measurement points within each fragment, indicating the high heterogeneity and complexity of the surfaces. Indeed, SEM-EDS is a non-destructive technique that allows for the examination of elemental composition with good spatial resolution. Cross-section preparation and destructive techniques were not allowed due to museum constraints. When analyzing degraded Ag-Cu fragments, significant variations in elemental concentrations- and consequently very high standard deviations- can be attributed to the intrinsic heterogeneity of the corroded samples. This results from the selective corrosion process, which leads to an uneven distribution of Ag and Cu. Additionally, surface roughness and corrosion layers can distort the EDS signal and hinder accurate quantification of the underlying metals [24–26].

HR Au-4f XPS reveals approximately 0.3 % at. of metallic Au, with two sharp peaks at 83.6 and 87.3 eV corresponding to the $Au4f_{7/2}$ and $Au4f_{5/2}$ components of metallic gold, respectively (Fig. 2) [27].

XPS detected low Pb contents (0.2–0.4 % at.). The Pb-4f doublet in the HR-XPS spectrum is ascribed to Pb(II) compounds (galena, PbS, or litharge, PbO) (Fig. 2), which can be related to the refining process [28]. Indeed, the primary silver ore in ancient China was argentiferous lead ore. The cupellation process resulted in the conversion of most lead to litharge and other impurities, leading to the production of over 95 wt% silver [29].

Silver embrittlement

The reliquary is in a highly brittle state with several missing pieces and deformation (*Fig. S6*). To investigate possible relations between the brittle condition and the microstructure, SEM analysis was conducted on the fragments, with the need of totally non-destructive techniques.

The back-scattered electron (SEM-BSE) images show the crack pattern along the tool mark profile, pitting and micrometric cracking both along and through the grain boundaries, the latter having a meandering and wiggly appearance (*Fig. S17*).

Fig. 3. SEM-BSE images of the section of the second component: the microcracks extend through the entire inner thickness of the foil; the back and front sides show a layered structure.

The embrittlement appears to likely result from a combination of intergranular and transgranular corrosion. As the present metalwork consists of Ag-Cu alloy foils, selective corrosion may have been facilitated by localized galvanic effects between the silver-enriched matrix (α-phase) and copper-enriched grain boundaries (β-phase) [8]. Furthermore, the cracks are preferentially located in the overworked zones, and the accumulation forms a mechanically weakened and corrosion-prone region. Therefore, the cracks could be mainly related to the previous intensive cold working, which left residual stresses and induced structural modification, according to the so-called stress corrosion cracking (SCC) [9]. Indeed, the indented decorations obtained by chasing and stamping might cause high residual strain hardening and give a meandering appearance to the grain boundaries. This created stress during cold working that was not removed by annealing. The residual stress, combined with soil pressure and the aggressive burial environment, resulted in severe cracking and subsequent embrittlement of the silver artefact. However, while SEM imaging provides morphological evidence, it may not be sufficient to fully elucidate the underlying mechanism of embrittlement. Additional metallurgical analyses – although destructive and thus not permitted in this study due to conservation constrains – could offer more conclusive insights into the causes of the embrittlement.

Corrosion products

Malachite, $CuCO_3{\bullet}Cu(OH)_2$, and mixed copper-zinc carbonates were identified by FTIR on the connecting component, base, parasol, and pole (3300–3400 cm^{-1}:OH stretching; 1400, 1550 cm^{-1}:CO_3^{2-} asymmetric stretching; 1040 cm^{-1}: coupled -CO_3^{2-} bending/asymmetric stretching; 960 cm^{-1}:OH bending; 880 cm^{-1}:CO_3^{2-} out-of-plane bending; 780 cm^{-1}:CO_3^{2-} in-plane bending). Additional bands in the mixed copper-zinc carbonates are at 830 cm^{-1} (-CO_3^{2-} out-of-plane bending), 1100 cm^{-1}, (-CO_3^{2-} symmetric stretching), and 730 cm^{-1} (-CO_3^{2-} in-plane bending); bands at 1400 and 1550 cm^{-1} are shifted to 1395 and 1500 cm^{-1} in the mixed copper-zinc carbonates (*Fig. S18*, spectra *g* and *h* in *Fig. S12*) [30,31]. The identification of Cu and Cu-Zn carbonates aligns with the alloy composition and the corrosion processes occurring in humid, carbonate-rich environments, resulting in differential re-

Table 1
Results of the characterization carried out on the front sides of the six micro-fragments (s1-s6). The crystalline phases and elemental compositions are obtained by XRPD and SEM-EDS point analysis (% at.), respectively. AgX refers to the mixed silver halide phases (Ag(Cl, Br)). The mean values and the standard deviations (in brackets) are reported in bold.

Sample	Location	Morphology	Crystalline phases	Ag (% at.)	Cu (% at.)	Au (% at.)	Cl (% at.)	Br (% at.)	S (% at.)	Ca (% at.)
s1	Central body	Coarse, patchy substrate. Presence of the terpene resin on both sides	Ag, AgX	0.12	-	–	0.10	-	–	-
				27.92	0.88		6.81	-		-
				0.36	-		0.28	-		0.10
				18.09	0.51		4.74	1.01		0.34
				54.71	-		37.58	-		-
				52.09	-		44.94	-		-
				31.21	-		24.22	5.00		-
				63.99	2.03		2.94	-		-
				18.56	-		16.89	2.01		0.34
				24.07	0.80		-	-		-
				28.46	-		26.58	2.68		-
				29.1 (20.8)	**1.1 (0.7)**	**–**	**16.5 (16.2)**	**2.7 (1.7)**	**–**	**0.3 (0.1)**
s2		Coarse, patchy substrate. Presence of the terpene resin on both sides	Ag, AgX, $CaCO_3$	6.65	0.64	-	1.25	0.31	0.12	7.55
				13.74	0.22	-	10.11	2.53	0.17	1.47
				7.35	0.80	-	0.29	-	0.14	7.15
				27.44	-	-	22.62	5.12	-	-
				37.4	0.81	0.38	0.69	-	-	-
				0.12	-	-	0.10	-	-	-
				25.98	-	-	21.39	2.01	-	0.38
				1.61	0.14	-	1.09	-	0.63	13.06
				27.71	-	-	22.68	4.34	-	-
				0.14	0.04	-	0.12	-	-	-
				22.03	-	-	17.79	2.03	-	-
				15.5 (18.2)	**0.4 (0.3)**	**0.4 (-)**	**8.9 (10.2)**	**2.7 (1.7)**	**0.3 (0.2)**	**5.9 (5.1)**
s3		Coarse, patchy substrate. Presence of the terpene resin on both sides	Ag, AgX	28.75	0.49	-	25.40	3.33	–	-
				0.89	14.87	-	0.70	-		-
				36.15	-	-	27.47	8.55		-
				1.15	12.18	-	0.83	0.27		-
				19.89	1.75	-	-	-		-
				0.43	1.99	0.43	-	-		-
				20.32	-	-	13.18	3.95		0.34
				40.43	-	-	24.73	9.78		-
				30.15	-	-	23.02	5.47		-
				19.45	1.03	-	-	-		-
				8.86	0.56	-	5.56	1.64		0.44
				18.7 (14.4)	**4.1 (5.9)**	**0.4 (-)**	**15.1 (11.5)**	**4.7 (3.5)**	**–**	**0.4 (0.1)**
s4		Compact and smooth. Presence of the terpene resin on both sides	Ag, AgX	1.36	-	-	0.20	-	–	–
	Base, first piece			29.96	0.73	0.33	1.09	-		
				26.64	0.69	0.24	1.09	-		
				44.02	6.65	-	-	-		
				32.58	1.48	-	-	-		
				21.23	-	-	19.64	1.74		
				26.0 (14.2)	**2.4 (2.9)**	**0.3 (0.1)**	**5.5 (9.4)**	**1.7 (-)**	**–**	**–**
s5		Compact and smooth.	Ag	38.85	0.54	-	0.84	-	-	-
	Base, third piece			3.23	0.18	-	0.39	0.07	0.14	0.17
				11.76	0.85	-	-	-	0.16	-
				29.56	-	-	11.59	4.99	-	-
				71.42	2.75	0.55	-	-	-	-
				4.71	0.20	-	-	-	-	7.38
				75.43	2.53	-	-	-	-	-
				33.6 (30.2)	**1.2 (1.2)**	**0.6 (-)**	**4.3 (6.3)**	**2.5 (3.5)**	**0.15 (0.01)**	**3.8 (5.1)**
s6		Coarse, patchy substrate. Presence of the terpene resin on both sides	Ag, AgX, $CaCO_3$	13.28	1.15	–	1.54	2.12	0.26	4.76
	Base, third piece			14.77	0.42		0.23	0.54	-	5.46
				7.7	1.02		2.11	1.43	-	7.66
				48.64	-		1.20	0.64	-	1.90
				0.29	-		0.16	-	-	1.04
				14.52	-		7.28	3.65	-	1.75
				3.68	-		0.30	0.23	-	17.66
				14.7 (16.0)	**0.9 (0.4)**	**–**	**1.8 (2.5)**	**1.4 (1.3)**	**0.3 (-)**	**5.8 (5.8)**

lease of Cu^{2+} and Zn^{2+}, and subsequent precipitations of carbonate phases [23].

Black patinas show high sulfur contents, related to sulphuration products (Ag_2S) (*Fig. S19*), and significant halide amounts (Cl: 16.8 % wt; Br: 8.6 % wt.) (*Fig. S20*).

Mixed silver (bromide substituted) halides, Ag(Cl, Br), were detected by XRPD in s1, s2, s3 and s6 (*Fig. S21* and *Fig. S22, Table S5*). *Table S6* displays the unit cell parameters calculated for AgCl and AgBr. All the values deviate from the corresponding references (5.54 Å for AgCl and 5.77 Å AgBr), confirming the presence of mixed silver (bromide substituted) halides [32]. No sulphur compounds were detected by XRPD, likely due to their amorphous nature or very thin layers.

XPS on the dark areas detected 1.4 %at. of sulfur and 0.9 % at. of chloride. HR-XPS in the silver region displays two characteristic peaks of Ag3d. The unresolved peak of Ag $3d_{5/2}$ has at least three components. The spectral feature at 367.2 eV can be assigned to AgO, AgCl, or Ag_2S. The peaks at 367.9 and 368.6 eV are distinc-

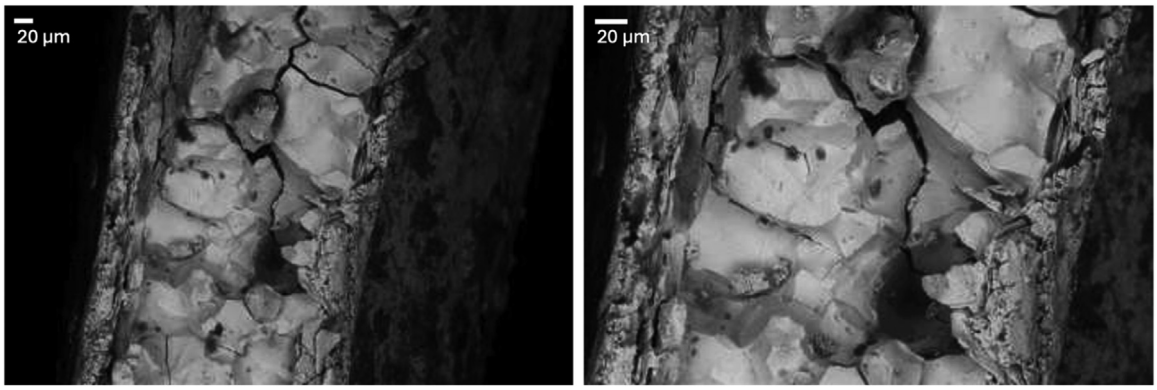

Fig. 3. displays the cracks running through the entire inner thickness of the foil and a large-grained substrate with brittle intergranular fracture. In addition, a top layered structure of about 20 µm thickness and delamination phenomena were observed on both the back and front sides.

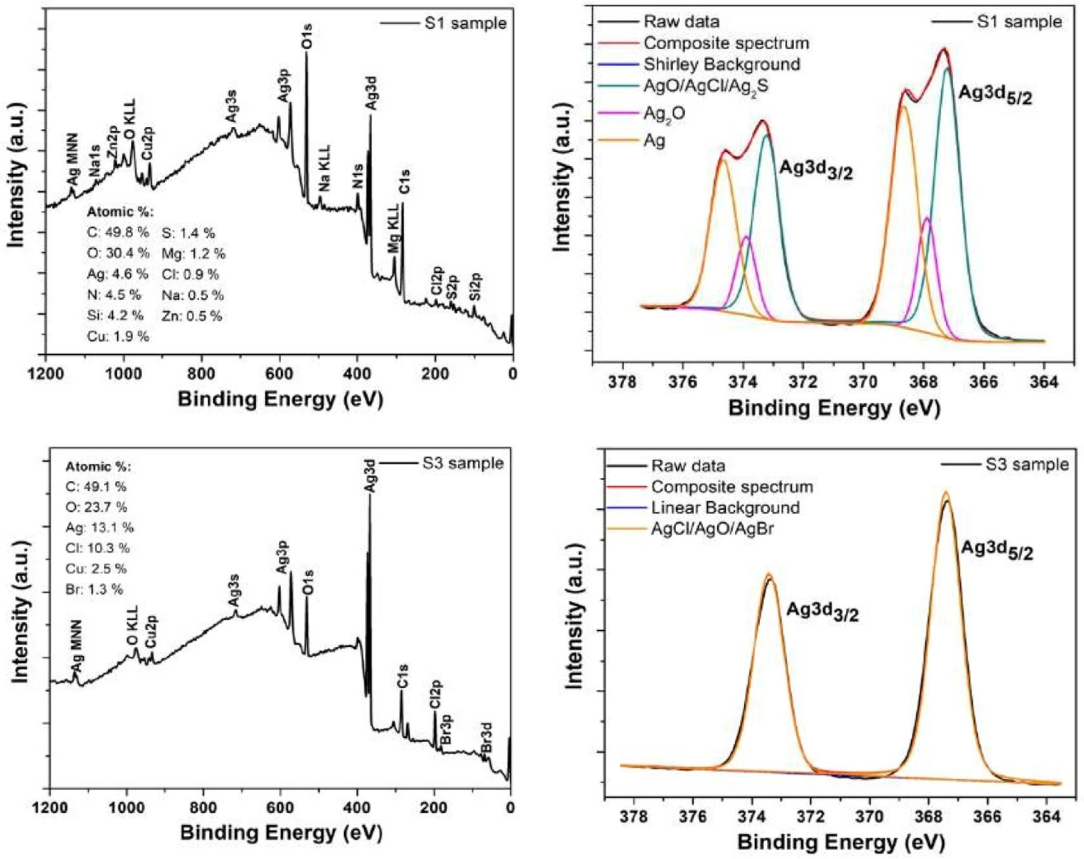

Fig. 4. Top graphs: survey XPS spectrum of fragment s1 and curve-fitting of the corresponding Ag3d HR-XPS spectrum. Bottom graphs: survey and high-resolution Agd3 XPS spectrum of sample s3 (point 7, front side): S was not detected in the dark patina.

tive for Ag_2O and Ag, respectively [33]. The high-resolution XPS spectrum of *s3* shows the doublet peak of Ag3d, attributable to AgBr/AgCl or AgO, consistent with the mixed silver (bromide substituted) halides detected by XRPD (Fig. 4) [34].

Thus, the common corrosion product a-Ag_2S (acanthite) is not the primary cause of the blackening. Instead, the dark patinas are also due to water-insoluble and photosensitive silver chloride and bromide [35]. This observation aligns with the dominant corrosion products found on ancient silver from marine or buried contexts, where halide-rich conditions prevail for extended periods. Moreover, the halide-based degradation products may result from previous improper surface cleaning [36].

Examining the coherence between the five components

The reliquary consists of five assembled components with a recurring repoussé phytomorphic motif, suggesting a possible deliberate visual and stylistic unity. The examination revealed that every piece exhibits unique decorative elements; some stylistic discrepancies in the decorative execution and material composition were identified, raising questions about their coherence and possible differences in the original production and/or restoration history.

The study points to partial coherence among the components:
Stylistic aspects

All five components have similar decorative themes, consistent with the Liao dynasty, but each piece displays distinct ornamental elements.

Material composition

A key inconsistency is the pole, which is made of brass, unlike the rest of the components, combined with modern glues identified at its extremities by FTIR. This indicates a later intervention, likely to stabilize or reassemble the structure.

Corrosion and chemical markers

The characterization of the micro-fragments, though limited to a small sample set and based exclusively on non-destructive techniques, provides the following evidence concerning the coherence question:

- Chloride content is higher in fragments from the central body (s1, s2, s3) compared to those from the first (s4) and third components (s5, s6) (*Fig. S23a*), likely reflecting different corrosion histories or conservation conditions.
- S/Ca ratios are similar between s2 (from the central body) and s5 and s6 (from the third component) and are higher than those of s1 and s3 (from the central body) and s4 (from the first component). Sulfur and calcium contents are positively correlated (*Fig. S23b*). This finding suggests some degree of chemical coherence between the third component and part of the body, but non uniformly across all body fragments.
- Fragments from the body (s1, s2, s3) have patchy surfaces, whereas s4 and s5 (from the base) show a uniform and smooth top layer (*Fig. S16*). S was not found in the dark patinas of fragments s1, s3, and s4, pointing to different corrosion processes or environments.

Thus, the findings suggest that the components seemed to be assembled to appear stylistically unified, but none of them are fully coherent in terms of alloy composition and corrosion products, suggesting partially different origins or environmental exposure. Some pieces, such as the third component and part of the central body, have similar S/Ca ratios. However, some inconsistencies, like the brass pole and different chloride levels between the central body and the first and third pieces, may indicate diverse steps in the reliquary production, conservation history or later restoration works.

Conclusions

A peculiar Chinese silver reliquary was investigated using a non-destructive approach. The early results allowed us to plan future conservation strategies and reveal the following key points:

- Material coherence: the micro-fragments from the central body show higher chloride contents and more alteration phases (silver halides and calcium carbonates) than other components. The pole is the only brass component, with modern glues at its extremities.
- New knowledge about metal-working of the Liao dynasty: the central body was cold-forged to form an octagonal prism and the ends were stitched together with silver threads. The base and roof were hammered from a single foil sheet.
- Conservation state: yellowing is due to terpenoid resins, likely from past restorations. Both sulphuration products and silver halides cause the foil darkening. Silver chloride and bromide suggest exposure to halide-rich environments, such as marine or burial contexts, and/or improper cleaning. The embrittlement appears to result from a combination of intergranular and transgranular corrosion, likely due to the burial environment and the intensive cold working involved in the manufacture.

Acknowledgments

The authors gratefully acknowledge the Museo d'Arte Orientale (MAO) in Turin, Italy.

This research did not receive any specific grant from funding agencies in the public, commercial, or not-for-profit sectors.

Supplementary materials

Supplementary material associated with this article can be found, in the online version, at doi:10.1016/j.culher.2025.07.013.

References

[1] S. Zacchetti, Chinese Buddhism from the origins to 581 CE, in: M. Sabattini, M. Scarpari (Eds.), La Cina vol. 2– L'età Imperiale Dai Tre Regni Ai Qing, Einaudi, Torino, 2010, pp. 429–490.
[2] H. Shen, Buddhist Relic Deposits from Tang (618-907) to Northern Song (960-1127) and Liao (907–1125) PhD Thesis, University of Oxford, 2000.
[3] H. Shen, Realizing the Buddha's dharma body during the Mofa period: a study of Liao Buddhist relic deposits, Artibus Asiae 61 (2) (2001) 263–303.
[4] H. Yang, Ancient Buddhist reliquaries in China and Korea, Chin. Archaeol. 10 (1) (2010) 184–195.
[5] T. Sen, Relic worship at the Famen Temple and the Buddhist World of the Tang Dynasty, in: Secrets of the Fallen Pagoda: Treasures from Famen Temple and the Tang Court, 2014, pp. 24–49.
[6] entry by M. Pirazzoli-t'Serstevens, *L'arte per la vita dell'Aldilà. Capolavori di arte antica cinese dalla collezione Meidaozhai*, 3 voll, in: M. Bussotti (Ed.), Fondazione Giovanni Agnelli, Torino, Fondazione Giovanni Agnelli, Torino, III, EFEO, Paris, 2002, pp. 200–201. entry by.
[7] D. Ashkenazi, H. Gitler, A. Stern, O. Tal, Archaeometallurgical characterization and manufacturing technologies of fourth century BCE silver jewelry: the Samaria and Nablus hoards as test case, Metallogr., Microstruct. Anal. 7 (4) (2018) 387–413.
[8] R.J.H Wanhill, Archaeological Silver embrittlement: a Metallurgical Inquiry, National Aerospace Laboratory NLR, Amsterdam, 2002.
[9] R.J.H. Wanhill, Stress corrosion cracking in ancient silver, Stud. Conserv. 58 (1) (2013) 41–49.
[10] H. Xiao, A probe into the manufacturing technology of gold and silver wares in Liao dynasty, J. Chifeng Univ. (Philos. Soc. Sci. Chin. Ed.) 1 (2021) 68–72 in Chinese.
[11] R. Zhao, Y. Kang, Influence of gold and silver technology of the Tang Dynasty on the gold and silver vessels in the Liao Dynasty, J. Inner Mongolia Normal Univ. (Philos. Soc. Sci.) 5 (2008) 118–121 in Chinese.
[12] D. Jalla, Relazioni sull'acquisizione di beni di arte orientale della Fondazione "Giovanni Agnelli, Archivio Musei Città Di Torino, Faldoni Acquisti Arte Orientale/Fondazione Agnelli, Torino, 2004.
[13] P.B. Welch, Chinese Art: a Guide to Motifs and Visual Imagery, Tuttle Publishing, Claredon, VT, 2012.
[14] S. Sung, A study on the gilt silver dharma relics pagoda excavated from the Heavenly palace of the *Qingzhou White Pagoda* of the Liao Dynasty, Korean J. Art Hist. 315 (2022) 277–323 (in Chinese).
[15] P. Tan, J. Yang, X. Ren, Technical features of a ninth-century silver vessel of southern China uncovered from Famen Monastery, Shaanxi province, Heritage Sci. 9 (1) (2021) 1–12.
[16] J.C.Y. Watt, A.E. Wardwel, When Silk was Gold: central Asian and Chinese Textiles, The Metropolitan Museum of Art, New York, 1997.
[17] H. Maryon, M. Cesai, La Lavorazione Dei metalli. Oreficeria, Argenteria e Tecniche Complementari, Ulrico Hoepli, Milano, 1998.
[18] R. Vinodh, C.M. Babu, R.Ravikumar A.Abidov, M. Palanichamy, E.Y. Choi, H.T. Jang, Synthesis and characterization of 1-octyl 2-cyano acrylate for wound healing applications, Int. J. Bio-Sci. Bio-Technol. 8 (1) (2016) 339–350.
[19] G. Socrates, Infrared and Raman Characteristic Group Frequencies. Tables and Charts, Wiley, Hoboken, NJ, USA, 2001.
[20] C. Innocenti, argenti Ori, in: gemme. Restauri dell'opificio Delle Pietre Dure, Mandragora, Firenze, 2007, p. 36.
[21] F. Zhao, Weaving, dyeing and embroidery of Liao dynasty silk from the white pagoda, Chin. Archaeol. 1 (1) (2001) 81- 84.
[22] M.H. Brooker, S. Sunder, P. Taylor, V.J. Lopata, Infrared and Raman spectra and X-ray diffraction studies of solid lead(II) carbonates, Can. J. Chem. 61 (1983) 494–502.
[23] D.A. Scott, Copper and Bronze in Art: corrosion, Colorants, Conservation, Getty publications, 2002.
[24] A. Mezzi, C. Riccucci, T. De Caro, E.M.M.A. Angelini, F. Faraldi, S. Grassini, V.K. Gouda, Combined use of SA-XPS, XRD and SEM+ EDS for the micro-chemical characterisation of Ag-based archaeological artefacts, Surf. Interface Anal. 46 (10–11) (2014) 801–806.
[25] G.M. Ingo, C. Riccucci, M. Pascucci, E. Messina, C. Giuliani, P. Biocca, L. Tortora, G. Fierro, G. Di Carlo, Combined use of FE-SEM+ EDS, ToF-SIMS, XPS, XRD and OM for the study of ancient gilded artefacts, Appl. Surf. Sci. 446 (2018) 168–176.

[26] A.M. Gójska, E.A. Mišta-Jakubowska, K. Kozioł, A. Wasilewski, R. Diduszko, The KX-ray intensity ratios as a tool of examination and thickness measurements of coating layers, Measurement 224 (2024) 113871.
[27] M.P. Casaletto, A. Longo, A. Martorana, A. Prestianni, A.M. Venezia, XPS study of supported gold catalysts: the role of Au0 and Au+δ species as active sites, Surf. Interface Anal. Int. J. Dev. Appl. Tech. Anal. Surf., Interfaces Thin Films 38 (4) (2006) 215–218.
[28] J.A. Taylor, D.L. Perry, An X-ray photoelectron and electron energy loss study of the oxidation of lead, J. Vac. Sci. Technol. A: Vac., Surf. Films 2 (2) (1984) 771–774.
[29] P.T. Craddock, J. Lang, in: Mining and Metal Production through the Ages, British Museum Press, London, 2003, pp. 198–206.
[30] M. Schmidt, H.D. Lutz, Hydrogen bonding in basic copper salts: a spectroscopic study of malachite, $Cu_2(OH)_2CO_3$, and brochantite, $Cu_4(OH)_6SO_4$, Phys. Chem. Miner. 20 (1993) 27–32.
[31] D. Stoilova, V. Koleva, V. Vassileva, Infrared study of some synthetic phases of malachite ($Cu_2(OH)_2CO_3$)–hydrozincite ($Zn_5(OH)_6(CO_3)_2$) series, Spectrochim. Acta Part A: Mol. Biomol. Spectrosc. 58 (9) (2002) 2051–2059.
[32] AgBr: JCPDS-International Centre for Diffraction Data No. 79-0149. AgCl: JCPDS-International Centre for Diffraction Data No. 85-1355.
[33] S. Glaus, G. Calzaferri, The band structures of the silver halides AgF, AgCl, and AgBr: a comparative study, Photochem. Photobiol. Sci. 2 (4) (2003) 398–401.
[34] G.B. Hoflund, Z.F. Hazos, G.N. Salaita, Surface characterization study of Ag, AgO, and Ag_2O using x-ray photoelectron spectroscopy and electron energy-loss spectroscopy, Phys. Rev. B 62 (16) (2000) 11126–11133.
[35] J.M. Cronyn, W.S. Robinson, in: The Elements of Archaeological, Routledge, London, 1990, pp. 230–231.
[36] R. Hedges, On the occurrence of bromine in corroded silver, Stud. Conserv. 21 (1) (1976) 44–46.